Original Article

CLINICAL AND EXPERIMENTAL VACCINE RESEARCH

Clin Exp Vaccine Res. 2025 Jan;14(1):10-22
https://doi.org/10.7774/cevr.2025.14.e10
pISSN 2287-3651·eISSN 2287-366X

Enhanced replication of a hepatitis A virus vaccine strain via adaptation in Vero cells

Sang Hwan Seo [1], **Jung-ah Choi** [1], **Mi Sun Kim** [1], **Eunji Yang** [1], **Sumin Choi** [2], **Dong Won Seo** [2], **Manki Song** [1]

[1]Science Unit, International Vaccine Institute, Seoul, Korea
[2]Gyeongbuk Institute for Bio Industry, Andong, Korea

OPEN ACCESS

Received: Nov 13, 2024
Revised: Nov 20, 2024
Accepted: Nov 20, 2024
Published online: Jan 22, 2025

Corresponding authors:
Dong Won Seo, PhD
Gyeongbuk Institute for Bio Industry, 5 Saneopdanji 2-gil, Pungsan-eup, Andong 36618, Korea.
Tel: +82-54-850-6852
Fax: +82-54-850-6801
Email: sdw1318@gib.re.kr

Manki Song, PhD
Science Unit, International Vaccine Institute, 1 Gwanak-ro, Gwanak-gu, Seoul 08826, Korea.
Tel: +82-2-881-1404
Fax: +82-2-881-1298
Email: mksong@ivi.int

Purpose: Hepatitis A virus (HAV) production has been limited by its slow replication rate and reliance on diploid cell lines like MRC-5, which present challenges in scalability, passage limitations, and serum-free culture conditions. This study aimed to develop an HAV vaccine strain with enhanced replication capacity.
Materials and Methods: We generated a reverse genetically modified HAV vaccine strain (RG-HAV) and adapted it to Vero cells through sequential culturing. Replication rates of RG-HAV and a commercially used strain, HM-175, were compared in Vero and MRC-5 cells. Nucleotide sequences, including coding and non-coding regions like the internal ribosomal entry site (IRES), were analyzed. Structural assessments included 3-dimensional modeling of IRES and relative codon deoptimization analysis of the capsid. Immunogenicity was evaluated by measuring HAV-specific antibody responses in mice.
Results: Vero-adapted RG-HAV achieved a 30-fold increase in production yield compared to initial transfection. In Vero cells, RG-HAV peaked at 15 days post-infection, compared to 20 days for HM-175. In MRC-5 cells, RG-HAV and HM-175 reached peak production at 10 and 15 days, respectively. RG-HAV produced over 5-fold more HAV in Vero cells and 8-fold more in MRC-5 cells than HM-175. Sequence analysis revealed nine amino acid differences in RG-HAV structural proteins and five nucleotide changes in the type III IRES region, potentially enhancing IRES functionality. Immunization with inactivated RG-HAV with alum hydroxide induced HAV-specific antibody responses in mice.
Conclusion: RG-HAV offers enhanced replication and production yields, supporting its potential in advancing HAV vaccine development.

Keywords: Hepatitis A virus; Vero cell; Reverse genetics; Internal ribosomal entry site; Codon

INTRODUCTION

Hepatitis A virus (HAV) belongs to the *Hepatovirus* genus within the *Picornaviridae* family and has a genome consisting of a positive-strand RNA [1]. HAV infection typically results in acute hepatitis A, with symptoms ranging from asymptomatic or mild in children to relatively severe or even fatal in adults [2]. The global burden of HAV infection is substantial, with estimates exceeding 100 million cases annually, approximately 1.5 million of which progress to clinical illness, resulting in 15,000–30,000

deaths worldwide each year [3]. The incidence of hepatitis A continues to rise globally [4]. Transmission of HAV primarily occurs via the fecal-oral route, often through direct contact with infected individuals or consumption of contaminated food or water [5]. Consequently, transmission is closely linked to inadequate hygiene and sanitation practices, particularly in low- and middle-income countries (LMICs). Despite favorable hygiene and sanitation standards in developed countries, HAV outbreaks still occur because of infected travelers from endemic LMICs and the importation of contaminated frozen food [6-10].

HAV vaccines are readily available and have demonstrated preventive efficacy exceeding 95% in both children and adults [11-13]. Therefore, the implementation of HAV vaccination programs represents a highly effective strategy for reducing the incidence of HAV infections. However, as of May 2019, routine immunization programs for HAV have been adopted or planned for children in only 34 countries. Additionally, despite being considered a vaccine-preventable disease, shortages in HAV vaccine supply have recurred during outbreaks, even in developed countries [14-17]. The limited introduction of HAV immunization programs and recurring supply shortages are primarily caused by production challenges and the resulting high vaccine costs. HAV is known to exhibit slow replication rates in all cell types, with the harvest of replicated HAV typically requiring approximately three weeks [18,19]. This slow replication rate is primarily due to inefficient translation mediated by the type III internal ribosomal entry site (IRES) of HAV [20-22]. Moreover, HAV does not inhibit host cell translation after infection, and the virus utilizes codons that deviate from those commonly used in host cells; this may also be the reason for its slow replication rate and low production yield [23-26]. Efforts to enhance HAV production systems by modifying the translational process in HAV to increase production yields and shorten harvest times offer a novel approach to address the limited introduction of HAV immunization programs and supply shortages experienced during HAV outbreaks.

Various approaches have been explored to improve HAV replication efficiency. Continued passage of HAV cultures has been attempted, leading to mutations in the 5′ untranslated region (UTR) and non-structural proteins [27-29]. These mutations resulted in the production of an attenuated HAV strain with a relatively rapid replication rate. However, subsequent studies in non-human primates revealed that these strains exhibited a loss of immunogenicity, rendering them unsuitable vaccine candidates [30]. Another trial involved the continued passage of HAV into fetal rhesus kidney (FRhK-4) cells in the presence of actinomycin to induce translational shutoff in the host cells [31]. This culture method induced mutations in the IRES region and altered the codon composition, resulting in the generation of fast-growing HAV strains in FRhK-4 cells. However, the replication rate and production yield of these new strains are not significantly higher than those of the wild-type HAV vaccine strain when cultured with vaccine-producing MRC-5 or Vero cells [32]. Furthermore, the ability of these new HAV strains to induce HAV-specific immune responses has not yet been investigated. As Vero cells are widely used in producing viral vaccines, HAV culture using Vero cells was also attempted in T75 flasks and bioreactors using microcarriers [33]. After 24 days of cultivation in a bioreactor, a 1:64 enzyme-linked immunosorbent assay (ELISA) titer of HAV was detected. In contrast, a 1:128 ELISA titer of HAV was detected in the T75 flask after 28 days of cultivation, indicating that the production yield of the bioreactor system was lower than that of the conventional T75 flask. Thus, further improvements in bioreactor culture systems are necessary to optimize the production of HAV vaccine strains.

MRC-5 cells, a diploid human fetal lung fibroblast line, are commonly used for the production of viral vaccine strains due to their high susceptibility to a broad range of viruses, including HAV. However, the production yield of HAV in MRC-5 cells has been relatively low, highlighting the need for optimization of the production process or the replacement of the cell line used for vaccine strain production. In contrast, Vero cells, derived from African green monkey kidney epithelium, present significant advantages for industrial-scale vaccine production due to their ability to proliferate indefinitely. Additionally, Vero cells have been extensively characterized and are widely recognized by regulatory authorities, such as the Food and Drug Administration and World Health Organization, for their suitability in viral vaccine manufacturing [34]. Therefore, transitioning the production cell line for HAV vaccine strain production from MRC-5 cells to Vero cells could address current yield limitations while offering notable advantages in both regulatory compliance and manufacturing scalability.

In this study, we demonstrated that the HAV vaccine strain generated via reverse genetics (RG-HAV) in Vero cells and subsequently adapted through sequential culture achieved an approximately 30-fold increase in production yield compared to the initial transfection of HAV mRNA. Additionally, RG-HAV exhibited superior production yield and replication rates in both MRC-5 and Vero cells compared to HM-175, a commercially used HAV vaccine strain. The immunization of mice with inactivated RG-HAV combined with an alum adjuvant induces an HAV-specific antibody response. These findings suggest that RG-HAV has significant potential as an improved HAV vaccine strain, offering enhanced efficiency of HAV vaccine production.

 https://doi.org/10.7774/cevr.2025.14.e10

MATERIALS AND METHODS

In vitro transcription

pUC57s vectors containing the 5′ and 3′ UTRs of HAV HM-175 (pUC57S-HAV-5′3′) and nucleotides containing the coding region of HAV HM-175 with *SbfI* and *PmeI* restriction enzyme sites at each end, respectively, were synthesized (Macrogen, Seoul, Korea). The coding region of HAV HM-175 was also inserted into a pUC57S-HAV-5′3′ vector (pUC57S-HAV). For *in vitro* transcription, plasmid DNA was linearized using *MluI* (R0198S; New England Biolabs [NEB], Ipswich, MA, USA) and *EcoRV* (R0195S; NEB), and the linearized DNA was purified using a QIAquick PCR & Gel Cleanup Kit (#28506; Qiagen, Hilden, Germany). Using the linearized plasmid DNA as a template, HM-175 RNA was generated *in vitro* using a TranscripAid T7 High-Yield Transcription Kit (K0441; Thermo Fisher Scientific, Waltham, MA, USA). The RNA product was purified using an RNeasy Mini kit (#74104; Qiagen), and its concentration was measured using a NanoDrop One instrument (Thermo Fisher Scientific) and electrophoresis.

HAV generation via reverse genetics

Vero cells were purchased from the Korean Ministry of Food and Drug Safety (KMFDS) and seeded at a density of 1.0×10^6 cells in a T-75 cell culture flask containing Eagle's Minimum Essential Medium (EMEM) (30-2003; ATCC, Manassas, VA, USA) supplemented with 10% fetal bovine serum (FBS, #12483020; Gibco, Waltham, MA, USA) and 1% Antibiotic-Antimycotic (#15240062; Gibco). The next day, Vero cells were washed twice with phosphate-buffered saline (PBS), and Opti-MEM (#31985070; Gibco) was added. Next, 7 μg of HM-175 RNA and 20 μL of Lipofectamine 3000 Transfection Reagent (#100022052; Invitrogen, Waltham, MA, USA) were mixed and used for treatment. After 4 hours of incubation at 32°C with 5% CO_2, the spent medium was replaced with EMEM (30-2003; ATCC) supplemented with 2% FBS and 1% antibiotics. After 10 days of incubation, the Vero cells were lysed by freezing and thawing. After centrifugation at 4,000 ×*g* for 10 minutes, the supernatant was collected. The collected supernatant samples were then analyzed using quantitative reverse transcription polymerase chain reaction (RT-PCR).

Adaptation of reverse genetically generated HAV (RG-HAV) in Vero cells

Vero cells were seeded at a density of 1.0×10^6 cells per well in T-75 cell culture flasks. After 24 hours, the cells were washed twice with PBS and then inoculated with a mixture comprising 1 mL of supernatant derived from transfected Vero cell lysates and 4 mL of EMEM (30-2003; ATCC) supplemented with 2% FBS (#12483020; Gibco) and 1% Antibiotic-Antimycotic (#15240062; Gibco). The inoculum was incubated with the Vero cells for 1 hour at 32°C in a 5% CO_2 atmosphere. Following the incubation, the inoculum was removed, and the cells were maintained in EMEM supplemented with 2% FBS and 1% Antibiotic-Antimycotic at 32°C in a 5% CO_2 incubator for 12 days. To harvest the amplified RG-HAV, the Vero cells were subjected to freeze-thaw cycles three times, and the supernatant was collected by centrifugation at 4,000 ×*g* for 10 minutes. The collected supernatant was subsequently used to re-infect fresh Vero cells under identical conditions, with each infection lasting 12 days. This process was repeated for a total of seven infection cycles to achieve amplification.

Purification of HAV

The supernatants from HAV cultures were harvested, filtered using 0.4-μm membrane filters, and incubated with 20%-PEG 8000 (P2139; Sigma-Aldrich, St. Louis, MO, USA) in 2.5 M NaCl (S9888; Sigma-Aldrich) for 16 hours. After that, the supernatant was centrifuged at 20,000 ×*g* at 4°C for 20 minutes. The resulting pellet was resuspended in 20 mL of PBS before incubation at 4°C for another 16 hours. The supernatant was then overlaid on a 30% Optiprep™ (Sigma-Aldrich) solution for ultracentrifugation at 150,000 ×*g* at 4°C for 4 hours. The resulting pellet was resuspended in 4 mL of PBS, and the resulting supernatant was overlaid on a 10%–50% Optiprep™ density gradient for ultracentrifugation 150,000 ×*g* at 4°C for 4 hours. Finally, the resulting opaque white band was collected and stored at –80°C for further analysis.

Quantitative RT-PCR

For HAV titration, viral RNA was extracted using a QIAamp Viral RNA Mini Kit (#52904; Qiagen). Quantitative PCR was performed using AgPath-ID One-Step RT-PCR Reagents (#4387424; Thermo Fisher Scientific) and a CFX96 Touch Real-Time PCR Detection System (Bio-Rad, Hercules, CA, USA). The probe and primer sequences used were as follows: probe, 5′-(FAM)-CTTAGGCTA-ATACTTCTATGAAGAGATGC-3′-(TAMRA); forward primer, 5′-GGTAGGCTACGGGTGAAA-3′; reverse primer, 5′-AACAACTCACCAATATCCGC-3′.

A standard template was used to calculate the genomic equivalent (GE) of HAV. Briefly, RT-PCR was conducted to linearize the pUC57s plasmid DNA to produce the HAV RNA standard. RT-PCR was performed using a Bioneer AccuPower® HotStart Pfu PCR PreMix (K2301; Bioneer, Daejeon, South Korea) and a CFX96 Touch Real-Time PCR Detection System (Bio-Rad). The primer sequences used were as follows: forward 5′-CGTTAATACGACTCACTATA GGGCTCTATAAGAACACTCATTTTCACGCTTTCTGTCTTCT-3′;

reverse 5′-AGTACCTCAGCGGCAAACAC-3′. Using the linearized DNA as a template, RNA was generated *in vitro* using a TranscripAid T7 High-Yield Transcription Kit (K0441; Thermo Fisher Scientific). The RNA product was purified using an RNeasy Mini kit (#74104; Qiagen), and its concentration was measured using a NanoDrop One instrument (Thermo Fisher Scientific) and electrophoresis. The RNA was aliquoted per 1×10^{10} copies to produce an HAV RNA standard stock. The GE of HAV was then calculated as follows:

$$\text{SQ Value} \times 12 \times \frac{60\ (Volume\ of\ RNA\ Extracted\ by\ Viral\ RNA\ Kit)}{140\ (Volume\ of\ Virus\ Sample\ for\ RNA\ Extraction)} \times \frac{1{,}000}{140} = GE/mL$$

Transmission electron microscopy (TEM)

For the morphological observation of RG-HAV, a formvar-coated, carbon-stabilized film grid was treated with glow discharge (15 mA for 60 seconds) to enhance its hydrophilicity. A drop of the purified HAV sample was deposited onto Formvar and carbon film on a 200 mesh Cu grid for 1 minute, followed by washing with distilled water. One drop of 2.5% uranyl acetate solution was then applied to the grid for 15 seconds. TEM images of HAV were obtained using a Talos L120C transmission electron microscope (Thermo Fisher Scientific) at an acceleration voltage of 120 kV.

Preparation of rotavirus

MA104 cells (CRL-2378.1; ATCC) were seeded at a density of 4.0×10^6 cells in a T-75 cell culture flask. One day after seeding, the flask was washed twice with serum-free Dulbecco's Modified Eagle Medium (DMEM, SH30243.01; Cytiva, Marlborough, MA, USA). The viruses, which were activated with 1 μg/mL TPCK-Trypsin (T1426; Merck, Rahway, NJ, USA), were added to MA104 cells at a multiplicity of infection (MOI) of 0.001 and incubated for 1 hour at 37°C in a 5% CO_2 incubator. After 1 hour, the inoculum was washed with serum-free DMEM, and the viruses were incubated with DMEM containing 0.5 μg/mL TPCK-Trypsin, 1% antibiotics (#15240062; Gibco), and 0.3% bovine serum albumin (BSA) (A0100-010; GenDEPOT, Katy, TX, USA) for 4 days at 37°C in a 5% CO_2 incubator. To obtain rotaviruses, the MA104 cells were frozen and thawed, and the supernatant was collected after centrifugation at 4,000 ×*g* for 10 minutes. Rotavirus was titrated via a plaque assay using an overlay medium containing 0.7% LE agarose (#32802; Thermo Fisher Scientific), DMEM (#12800017; Gibco), and 0.5% TPCK-Trypsin (T1426; Merck) at 37°C in a 5% CO_2 incubator.

ELISA for HAV

Sandwich ELISA was conducted to detect HAV antigens. ELISA plates were initially coated with pooled HAV serum (AccuSet HAV Mixed Titer Performance Panel, 0820-0443, Batch 10536946; SeraCare Life Sciences Inc., Milford, MA, USA) at a dilution of 1:5,000 in Dulbecco's PBS (DPBS) (SH30028.02; HyClone, Logan, UT, USA) and incubated at room temperature (RT: 20°C–24°C) for 18 hours. Following 3 washes with PBS containing 0.05% Tween 20 (P1379; Sigma-Aldrich), 200 μL of a starting block blocking buffer (#37538; Thermo Fisher Scientific) was added to each well, and incubated at RT for 2 hours. Subsequently, after one wash with PBS containing 0.05% Tween 20 (P1379; Sigma-Aldrich), 100 μL of the supernatant from the infected cells was seriallydiluteddispensed into each well, and incubated at 37°C for 2 hours. Following 3 washes with PBS containing 0.05% Tween, 100 μL of anti-HAV-horseradish peroxidase antibody (Vant-Lsx014; Creative Biolabs, Shirley, NY, USA) (1:100) was added to the wells and incubated at 37°C for 75 minutes. After five washes with PBS containing 0.05% Tween 20 (P1379; Sigma-Aldrich), 100 μL of tetramethylbenzidine (TMB) substrate solution (5120-0070; SeraCare Life Sciences Inc.) was added to each well and incubated at RT for 15 minutes. The enzymatic reaction was terminated by adding 100 μL of TMB stop solution (5150-0021; SeraCare Life Sciences Inc.), and the absorbance was measured at 450 nm using a SpectraMax iD3 instrument (Molecular Devices, San Jose, CA, USA). A standard curve was generated using diluted inactivated HAV to determine the number of HAV antigen units (A30; Mediagnost, Reutlingen, Germany).

Growth curve generation

To obtain viral growth curves, MRC-5 (purchased from the KMFDS) and Vero cells were cultured at densities of 2×10^6 and 5×10^6 cells, respectively, in T-75 cell culture flasks. Following a one-day incubation at 32°C and 5% CO_2, the cells were subjected to infection with a MOI of 10 of either HM-175 (VR-1402; ATCC) or RG-HAV in 5 mL of EMEM (30-2003; ATCC) supplemented with 2% FBS (26140-079; Gibco) and 1% Antibiotic-Antimycotic (15240-602; Gibco). After a one-hour incubation at 32°C with 5% CO_2, an additional 10 mL of EMEM containing 10% FBS and 1% antibiotics was added to the cells. The plates were then incubated for 20 days, replacing half the spent medium with fresh culture medium every 10 days. Viral titers were assessed via quantitative RT-PCR, as described above, and ELISA specifically targeting HAV, as described below.

Analysis of the nucleotide sequence of RG-HAV via rapid amplification of cDNA ends (RACE)-Seq

HAV RNA was extracted using a QIAamp Viral RNA Mini Kit (#52904; Qiagen), according to the manufacturer's instructions. Primer design (**Supplementary Table 1**) and sequencing were performed by Cosmo Genetech Co., Ltd. (Gwangju, Korea).

 https://doi.org/10.7774/cevr.2025.14.e10

For 3′ RACE PCR, a poly(A) tail was added to the HAV RNA by incubating it with *Escherichia coli* poly(A) polymerase (M051S; Enzynomics, Daejeon, Korea) at 37°C for 30 minutes. The reaction was terminated by heating the samples at 65°C for 20 minutes. Reverse transcription was performed using QT-RT primers. Sequential amplification was performed using the primers Q0-R and QI-R and gene-specific primers 3raceF1 and 3raceF2 to generate sequence-specific products. The sequencing of PCR products was conducted using HPA1-specific forward primers, and sequence assembly was performed using DNAStar SeqMan® software (DNASTAR Inc., Madison, WI, USA).

For 5′ RACE PCR, first-strand cDNA was synthesized using a 5′-phosphorylated RT-primer (5race-PR2). Hybrid RNA was treated with RNase H (M0297S; NEB) at 37°C for 1 hour. The single-strand cDNA was then ligated using T4 DNA ligase (M0204S; NEB) in the presence of 50% PEG8000 and ATP, incubated at RT (20°C–24°C) for 18 hours. Sequential amplification was performed using specific primers (5raceF7, 5raceR5, 5raceF8, and 5raceR6). The PCR products were sequenced using HPA1-specific primers and the sequences were assembled as described above.

Prediction of IRES structure

The mfold algorithm available on the mfold Web Server (http://unafold.rna.albany.edu) was used to describe the secondary structure of the IRES.

Bioinformatics analyses of the relative codon deoptimization index (RCDI)

The RCDI compares the match between the codon usage of HAV and its host. Although HAVs were grown in Vero cells, which came from rhesus macaques, we chose the *Macaca mulatta* codon usage because of the very similar codon usage between rhesus macaque and *M. mulatta* in the Codon Usage Database (*M. mulatta* n=1,051; http://www.kazusa.or.jp/codon/). The RCDI was calculated with parameters 15 codon-sliding and 100 codon-window using a public server (http://genomes.urv.es/CAIcal/RCDI/). The RCDI values indicate the rate of viral gene translation in the host genome. One RCDI indicates that the codon usage by the virus and host is similar.

Inactivation of RG-HAV

HAV was inactivated via incubation with 250 μg/mL of formaldehyde (#47608; Sigma-Aldrich) for 7 days at 37°C. To remove the formaldehyde, the mixture of HAV and formaldehyde was purified by performing untrafiltration/diafiltration (UF/DF) with PBS (#10010023; Gibco) 5 times using the 100-kDa cutoff Hollow fiber cartridge (UFP-100-E-H42LA; Cytiva) of an AKTA flux s instrument (Cytiva).

Immunogenicity assessment of RG-HAV in mice

Six-week-old female BALB/c mice were procured from Koatech (Pyeongtaek, Korea). To assess the immunogenicity of RG-HAV, the mice were intramuscularly immunized with inactivated RG-HAV (2×10^4 GE) adjuvanted with alum hydroxide (AH; Invitrogen) twice, with a 2-week interval between each dose. AH was diluted at 1:7 of the total volume, containing 0.0625 mg of aluminum hydroxide. Blood samples were obtained from the retro-orbital plexus of the anesthetized mice 2 weeks after the first and second immunizations. The collected blood samples were then analyzed for HAV-specific antibody titers using ELISA, following the procedure described below. All mouse experiments were conducted following the protocols approved by the Institutional Animal Care and Use Committee (IACUC) of the International Vaccine Institute, adhering to the guidelines outlined in IACUC PN 2022-008.

ELISA detection of anti-HAV IgG

The inactivated HAV (Bio-Rad), initially at a concentration of 206 μg/mL, was diluted to 2 μg/mL using PBS (Thermo Fisher Scientific), 100 μL of the solution was coated onto each well of 96-well plates (Thermo Fisher Scientific), and the plates were incubated overnight at 4°C. After incubation, the wells were washed three times with a wash buffer (PBS with 0.05% Tween-20; Sigma-Aldrich), and 100 μL blocking buffer (2% BSA [Sigma-Aldrich] in PBS containing 0.05% Tween-20) was added to each well. The plates were then incubated for 1 hour at 37°C. Mouse serum samples were prepared by diluting them 1:30 in an antibody buffer (0.5% BSA in PBS containing 0.05% Tween-20). Post-blocking, the wells were washed thrice with the wash buffer, and 100 μL of the prepared serum samples were loaded per well, followed by serial 1:5 dilutions. The plates were then incubated overnight at 4°C. Following another round of washing with PBS, goat anti-mouse HRP-labeled IgG (Southern Biotech, Birmingham, AL, USA), diluted 1:3,000 in antibody buffer, 100 μL was added into each well of the plates, and incubated for 1 hour at 37°C. After incubation, the wells were washed thrice with the wash buffer, and 100 μL of a TMB solution (Millipore, Burlington, MA, USA) was added per well for color development. The reaction was terminated by adding 100 μL of 0.5 N HCl (Merck) per well. The absorbance values were measured at 450 nm using a SpectraMax™ ABS Plus microplate reader (Molecular Devices), and the data were analyzed using SoftMax Pro 7.1.0 software (Molecular Devices) to determine the log2 titers.

RESULTS

Generation of HAV vaccine strains in Vero cells via reverse genetics

To generate an HAV vaccine strain in Vero cells via reverse genetics, plasmid DNA containing the full HM-175 sequence was generated (**Fig. 1A**). Subsequently, this plasmid DNA was linearized via enzyme cutting, followed by the isolation of the correct band post-electrophoresis (**Fig. 1B**) to serve as a template for *in vitro* transcription. Through this process, the RNA encoding the full-length HM-175 sequence was synthesized (**Fig. 1C**). Ten days after the transfection of HM-175 RNA into Vero cells, HAV RNA was successfully detected. Therefore, an HAV vaccine strain was generated via reverse genetics in Vero cells.

Adaptation of the HAV vaccine strain in Vero cells

A sequential re-infection process was performed to assess the infectivity of the HAV vaccine strain generated via reverse genetics (RG-HAV) in Vero cells and induce RG-HAV adaptation in Vero cells (**Fig. 2A**). Twelve days after post-reinfection with the initially generated RG-HAV in Vero cells, elevated titers of RG-HAV were observed in the supernatant, indicating the infectivity of the RG-HAV particles. Subsequent re-infections resulted in a progressive increase in the harvested viral titers, which persisted until the sixth re-infection. Following the seventh re-infection with RG-HAV, a marginal decrease in the viral titer was noted, prompting the cessation of the adaptation process. TEM analysis of the Vero cell-adapted RG-HAV samples revealed the presence of HAV particles with a uniform, non-enveloped morphology (**Fig. 2B**). The ELISA results for RG-HAV demonstrated a correlation between the absorbance values and RG-HAV concentrations. In contrast, the absorbance values for various concentrations of rotavirus, a negative control, were similar to those of the blank (**Fig. 2C and D**), confirming that RG-HAV contains the surface antigens of HAV. Collectively, these results indicate that we generated RG-HAV with an enhanced production yield in Vero cells.

Comparison of RG-HAV with HM-175 in terms of growth kinetics

Given the accelerated growth rate facilitated by adaptation to Vero cells, a comparative analysis was performed between RG-HAV and HM-175, an HAV vaccine strain, to elucidate their respective growth kinetics. Growth kinetics were assessed via RT-PCR and ELISA using cell supernatants following the infection of MRC-5 or Vero cells with 10 MOI of RG-HAV or HM-175. Morphological changes indicative of cytopathic effects (CPEs) were observed in both MRC-5 and Vero cells at 10 days post-RG-HAV infection, resembling

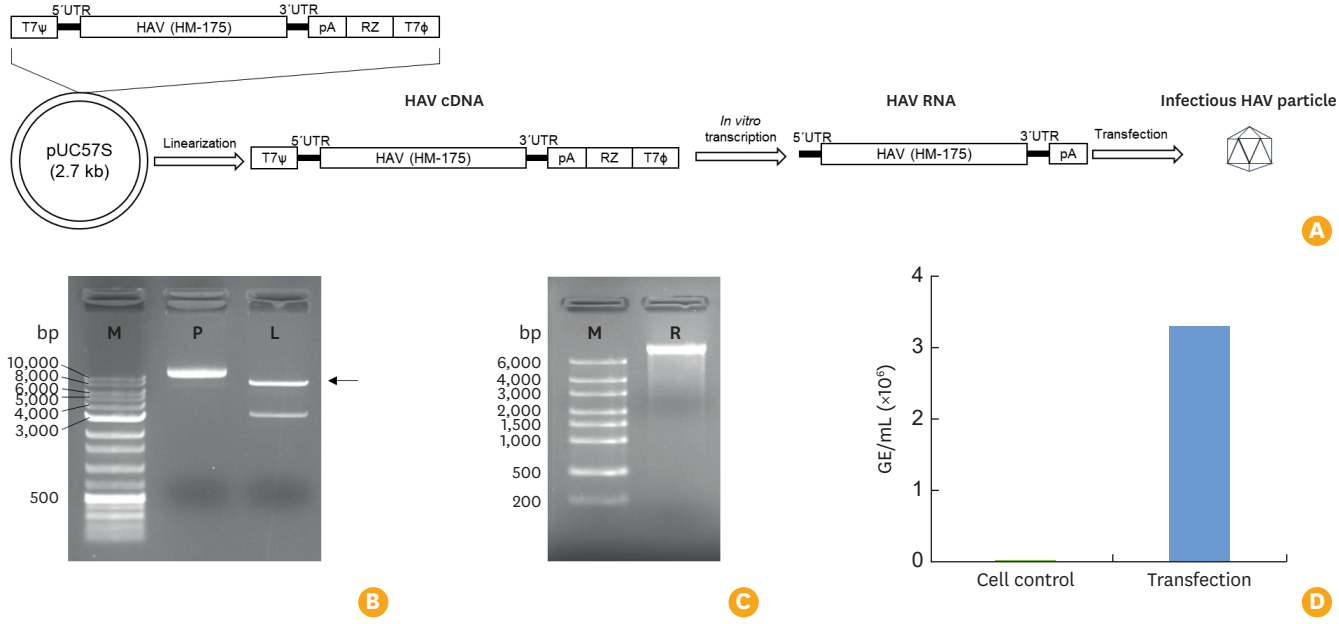

Fig. 1. Generation of an HAV vaccine strain using reverse genetics in Vero cells.
(A) Schematic of generating an HAV vaccine strain using reverse genetics. (B) pUC57S-HAV was linearized, and HAV cDNA was isolated after electrophoresis (M: DNA size marker, P: pUC57-HAV, L: linearized HAV cDNA [arrow]). (C) *In vitro* transcription product (*HAV* RNA) isolated after electrophoresis (M: RNA size marker, R: *HAV* RNA generated *in vitro*). (D) Ten days after transfection of *HAV* RNA in Vero cells, the generated HAV was assessed using quantitative RT-PCR (cell control: no HAV RNA transfected sample).
HAV, hepatitis A virus; RT-PCR, reverse transcription polymerase chain reaction; GE, genomic equivalent.

 https://doi.org/10.7774/cevr.2025.14.e10

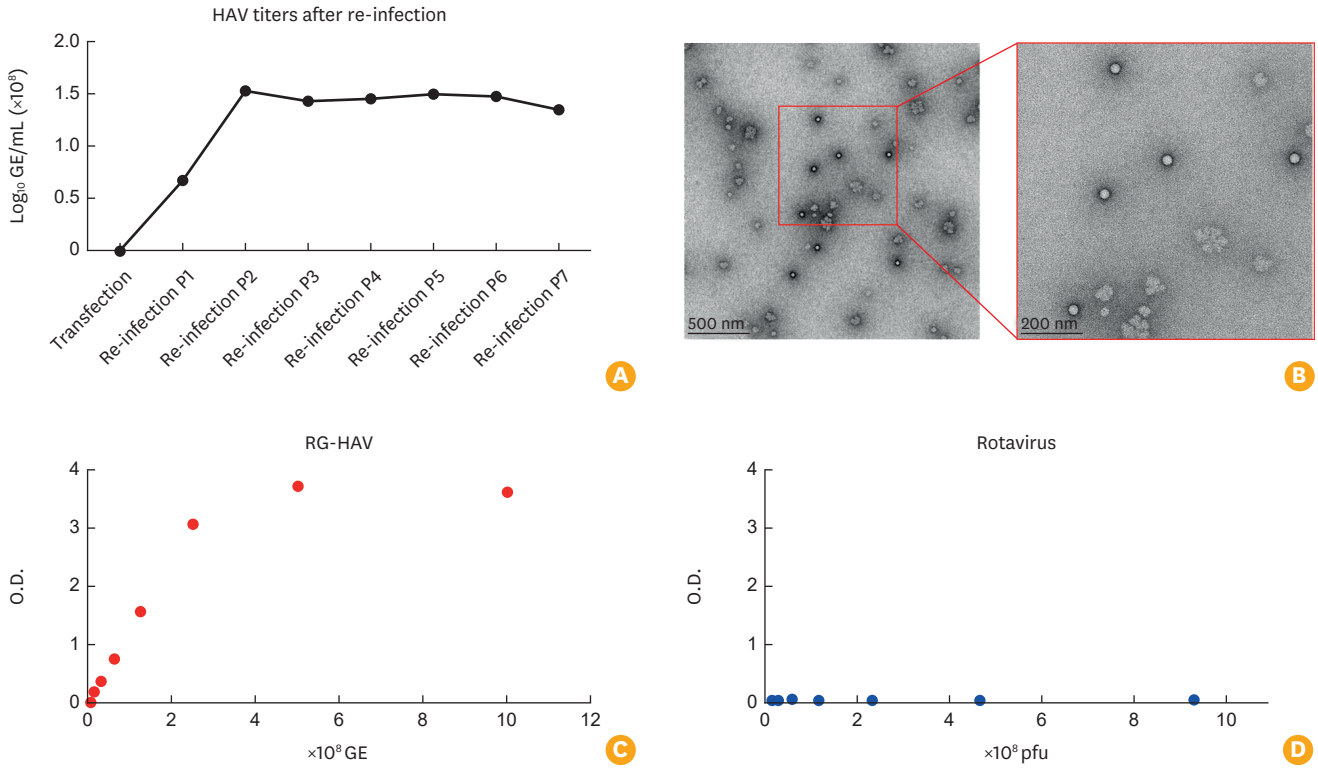

Fig. 2. Adaptation of the HAV in Vero cells.
(A) RG-HAV was re-infected in Vero cells serially. The samples collected 12 days after re-infection were analyzed using quantitative RT-PCR. (B) Transmission electron microscopy images of RG-HAV. The image on the right is a magnified view of the red box in the left image. ELISA results for RG-HAV (C) and rotavirus (D). HAV, hepatitis A virus; RG-HAV, hepatitis A virus vaccine generated via reverse genetics; RT-PCR, reverse transcription polymerase chain reaction; ELISA, enzyme-linked immunosorbent assay; GE, genomic equivalent; O.D., optical density.

fast-growing cytopathic strains (**Supplementary Fig. 1A and B**) [35-37]. However, HM-175-infected MRC-5 or Vero cells exhibited no discernible morphological changes until 20 days post-infection.

In RG-HAV-infected MRC-5 cells, HAV production peaked at 10 days post-infection, with a viral titer of 9.52 $\log_{10}$ GE/mL (**Fig. 3A**). HAV production reached 9.27 $\log_{10}$ GE/mL at 20 days post-RG-HAV infection. In contrast, HAV production in HM-175-infected MRC-5 cells did not peak at 10 days post-infection (8.59 $\log_{10}$ GE/mL), but at 15 days post-infection, with a viral titer of 9.18 $\log_{10}$ GE/mL. Twenty days post-MH-175 infection, HAV production was 8.95 $\log_{10}$ GE/mL. Consequently, RG-HAV demonstrated an 8.46-fold higher production yield at 10 days post-infection, 2.12-fold higher yield at 20 days post-infection, and 2.17-fold higher yield at its peak production than HM-175 in MRC-5 cells.

In RG-HAV-infected Vero cells, HAV production was 9.16 $\log_{10}$ GE/mL at 10 days post-infection, peaking at 15 days post-infection at 9.23 $\log_{10}$ GE/mL, and was 9.18 $\log_{10}$ GE/mL at 20 days post-infection (**Fig. 3B**). In HM-175-infected Vero cells, HAV production was 8.07 $\log_{10}$ GE/mL at 10 days post-infection, 8.50 $\log_{10}$ GE/mL at 15 days post-infection, and peaked at 9.03 $\log_{10}$ GE/mL at 20 days post-infection. Consequently, the yield of RG-HAV was 12.30-fold higher at 10 days post-infection, 5.36-fold higher at 15 days post-infection, 1.44-fold higher at 20 days post-infection, and 1.61-fold higher at the peak production point compared to HM-175 in Vero cells.

Consistent with the RT-PCR findings, ELISA results showed peak HAV antigen titers at 10 days post-RG-HAV infection in MRC-5 cells, whereas peak titers were observed at 15 days post-RG-HAV infection in Vero cells (**Fig. 3C and D**). Notably, HAV antigen titers were consistently higher in RG-HAV-infected MRC-5 cells at all measured time points than their HM-175-infected counterparts. However, in RG-HAV-infected Vero cells, the peak HAV antigen titer was higher at 20 days post-HM-175 infection than at 10 days post-RG-HAV infection, which was potentially influenced by CPE post-RG-HAV infection in Vero cells. These findings suggest that RG-HAV exhibits superior replication kinetics than HM-175 in both Vero and MRC-5 cells, highlighting its potential as a vaccine candidate.

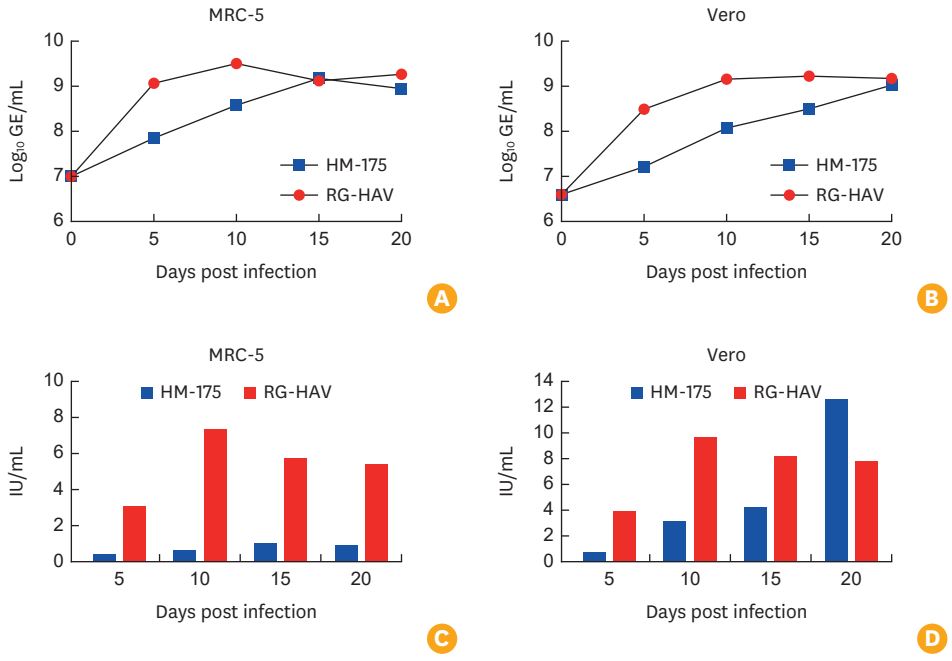

Fig. 3. Comparison of the growth kinetics of RG-HAV and HM-175 in MRC-5 and Vero cells.
Following infection with 10 MOI of either RG-HAV or HM-175 in MRC-5 or Vero cells, the growth kinetics were evaluated by subjecting the culture supernatants to RT-PCR (A, B) and ELISA (C, D).
RG-HAV, hepatitis A virus vaccine generated via reverse genetics; MOI, multiplicity of infection; RT-PCR, reverse transcription polymerase chain reaction; ELISA, enzyme-linked immunosorbent assay; GE, genomic equivalent.

Sequence analysis of structural proteins and IRES in RG-HAV

Previous reports demonstrated that HAV adaptation can alter nucleotide sequences, reducing immunogenicity [27-30]. Therefore, we initially analyzed the nucleotide and amino acid sequences of RG-HAV. Thirteen nucleotide changes were identified in the structural region (P1) of RG-HAV (**Fig. 4A and B**). These nucleotide alterations resulted in nine amino acid substitutions: T590K in VP3; N982D, S1016P, T1017N, V1018E, and T1019S in VP1; and K1092N, I1103M, and T1202A in 2A. Notably, these amino acid changes were not located within antigenic regions or major neutralizing epitopes (**Fig. 4C**), suggesting that the observed amino acid substitutions were unlikely to affect the immunogenicity of RG-HAV.

In a previous study, RG-HAV exhibited a superior replication rate than HM-175. Since the replication rate of HAV is primarily associated with its IRES activity, we also analyzed the IRES nucleotide sequences of RG-HAV. Five nucleotide changes were identified in the IRES of RG-HAV compared to that of HM-175 (**Fig. 5A**). Structural prediction revealed a distinct RNA conformation in the nucleotide-changed region (positions 323–324, AA>GC) between HM-175 and RG-HAV (**Fig. 5B and C**). RCDI analysis identified 8 regions in RG-HAV that exhibited lower RCDI values compared to HM-175 (codon positions 15–30, 195–225, 525–540, 645–675, 705–720, 750–780, 810–840, and 870–900) (**Fig. 5D**), indicating that RG-HAV uses more optimized codons than HM-175. These data suggest that the enhanced production yield of RG-HAV is likely associated with the adoption of more optimized codon usage than HM-175 and presumably due to improved IRES activity resulting from alterations in the IRES domain.

Assessment of RG-HAV immunogenicity in mice

To investigate whether RG-HAV could induce HAV-specific antibody responses, mice were immunized twice at 2-week intervals with inactivated RG-HAV and AH or PBS (as a negative control) (**Fig. 6A**). Sera collected 13 and 27 days after the first immunization were analyzed for HAV-specific antibody titers using ELISA. Thirteen days after the initial immunization, mice immunized with inactivated HAV and AH exhibited significantly higher anti-HAV antibody titers than mice injected with PBS (**Fig. 6B**). Booster immunization with inactivated HAV and AH further increased HAV-specific antibody induction. These results indicate that inactivated RG-HAV induces HAV-specific antibody responses in mice.

DISCUSSION

Owing to their inefficient translation efficiency, large-scale

 https://doi.org/10.7774/cevr.2025.14.e10

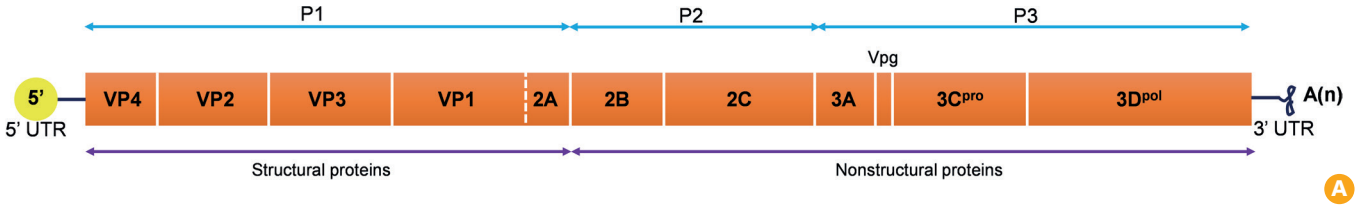

A

Region	nucleotide position	nucleotide HM-175	nucleotide RG-HAV	amino acid position	amino acid HM-175	amino acid RG-HAV
P1						
VP2	1001	T	C			
VP3	1755	C	A	590	T (Threonine)	K (Lysine)
VP1	2266	A	G			
	2698	C	T			
	2764	T	C			
	2930	A	G	982	N (Asparagine)	D (Aspartic acid)
	3032	T	C	1016	S (Serine)	P (Proline)
	3036	C	A	1017	T (Threonine)	N (Asparagine)
	3039	T	A	1018	V (Valine)	E (Glutamic acid)
	3041	A	T	1019	T (Threonine)	S (Serine)
2A						
	3262	A	T	1092	K (Lysine)	N (Asparagine)
	3295	A	G	1103	I (Isoleucine)	M (Methionine)
	3590	A	G	1202	T (Threonine)	A (Alanine)

B

C

Fig. 4. Analysis of the nucleotide and amino acid sequences of RG-HAV.
(A) Structure of the HAV genome. (B) Variations in the nucleotide and amino acid sequences between RG-HAV and HM-175. (C) Location of the altered amino acids in RG-HAV (Red box: epitope within the antigenic region; Yellow box: epitope with neutralizing antigenic properties; Green box: C-terminal domain; Yellow highlights indicate the altered amino acids).
RG-HAV, hepatitis A virus vaccine generated via reverse genetics; HAV, hepatitis A virus; UTR, untranslated region.

production of HAV vaccine strains is challenging. Additionally, MRC-5, a human diploid cell line used in HAV vaccine production, has limitations in large-scale culture. To address these issues, we generated RG-HAV in Vero cells and demonstrated an improved production yield. Comparative studies indicated that RG-HAV exhibited a higher replication rate than HM-175 in both MRC-5 and Vero cells. Thus, culturing the RG-HAV strain in Vero and MRC-5 cells is a

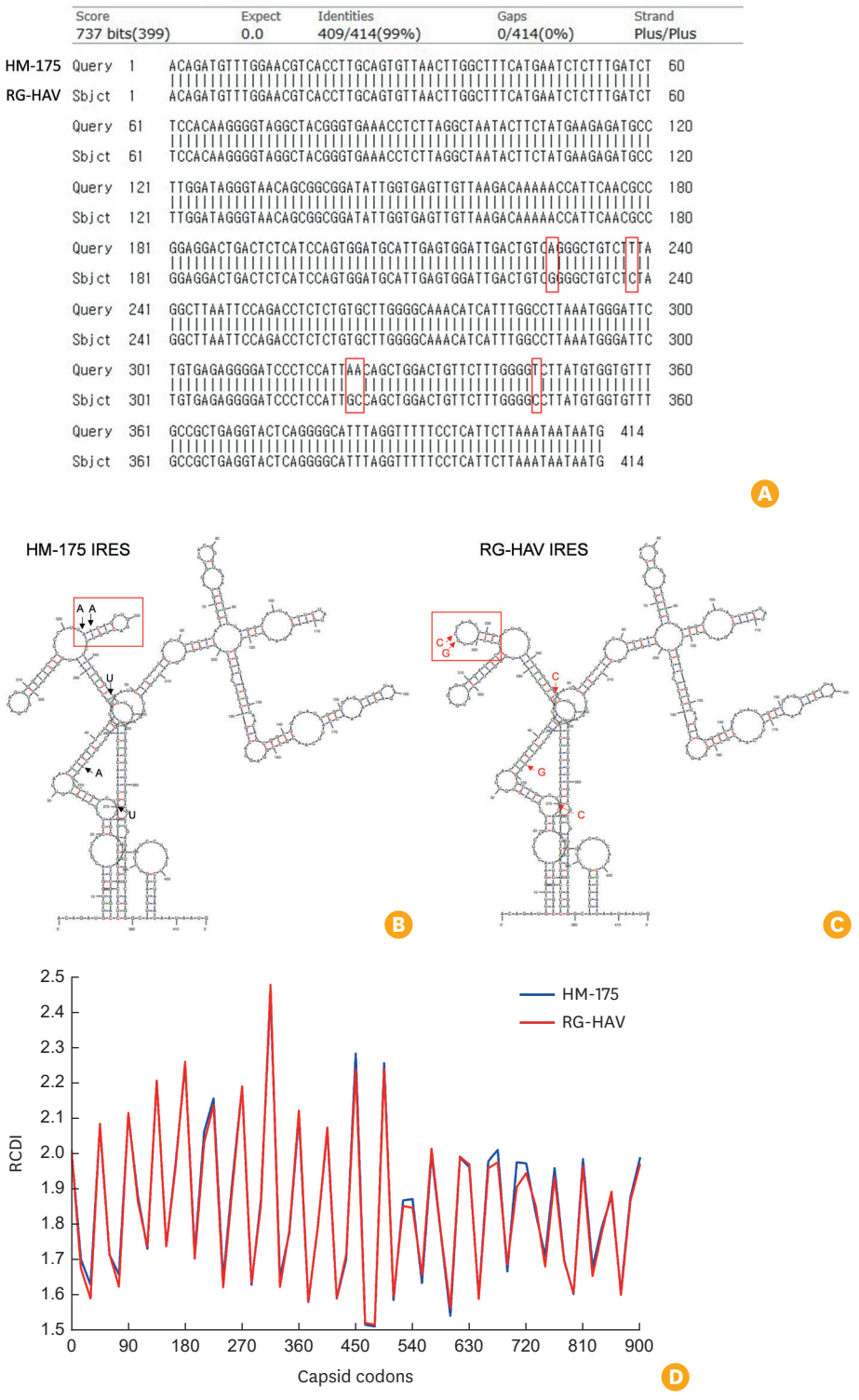

Fig. 5. Comparison of the IRES between HM-175 and RG-HAV.
(A) Comparative analysis of the nucleotide sequences of the IRES between HM-175 and RG-HAV. The predicted secondary structures of the IRES in HM-175 (B) and RG-HAV (C) are shown. (D) Relative codon deoptimization index of the capsid of HM-175 and RG-HAV.
IRES, internal ribosomal entry site; RG-HAV, hepatitis A virus vaccine generated via reverse genetics; RCDI, relative codon deoptimization index.

 https://doi.org/10.7774/cevr.2025.14.e10

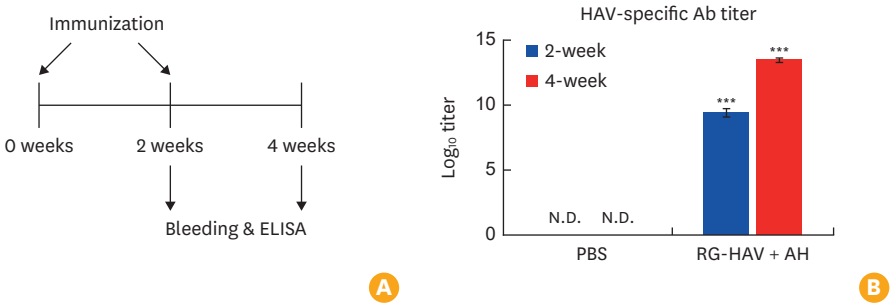

Fig. 6. Immunogenicity assessment of RG-HAV.
(A) Six-week-old BALB/c mice were intramuscularly immunized with RG-HAV (2×10^4 GE) with AH or PBS twice at a 2-week interval. (B) Sera were collected two weeks after primary and booster immunization, and the HAV-specific Ab titers were analyzed using ELISA.
RG-HAV, hepatitis A virus vaccine generated via reverse genetics; GE, genomic equivalent; AH, alum hydroxide; PBS, phosphate-buffered saline; HAV, hepatitis A virus; ELISA, enzyme-linked immunosorbent assay; N.D., not detected.
***$p<0.001$.

promising method for large-scale vaccine production.

The use of Vero cells for viral vaccine production is well-established and widely accepted by regulatory authorities because of their reliability. Vero cells have also consistently demonstrated their effectiveness in generating high-quality viral vaccines for many years. Nevertheless, research on enhancing cell culture systems for viral vaccine production is ongoing [34]. Notably, innovative approaches such as bioreactors that incorporate carriers to expand the available surface area for cell growth are under investigation. These advancements aim to improve productivity and reduce production costs, which are crucial factors in the global vaccine demand. Cell culture-based vaccine manufacturing continues to face challenges in producing large volumes of viruses while keeping costs manageable, particularly in the context of global health needs and the imperative to provide vaccines in low-income countries. Addressing these challenges requires significant innovations. In this regard, developing a high-yield recombinant HAV strain (RG-HAV), along with an optimized Vero cell culture process, represents a promising advancement. This combination has the potential to significantly improve production efficiency and address the current limitations of HAV vaccine production.

Our comparative growth study revealed that RG-HAV produced higher HAV yields than HM-175 in Vero and MRC-5 cells (**Fig. 3**). Therefore, RG-HAV has potential advantages in current commercial HAV production systems. In MRC-5 cells, RG-HAV-infected cultures reached peak virus production 10 days post-infection, with yields declining on days 15 and 20. Similarly, peak virus production was observed 15 days post-infection in Vero cells, after which the yields also decreased. The observed decline in HAV production beyond these peak times was likely due to reduced cell viability, as CPE became evident at 10 days post-RG-HAV infection in both cell types under T75 culture conditions. Therefore, optimization of the culture conditions in Vero and MRC-5 cells is recommended to enhance RG-HAV production. Further investigations adjusting these conditions could leverage the high production efficiency of the RG-HAV strain, potentially leading to improved yields and more effective production processes than the ones reported in this study.

Sequential culture of RG-HAV in Vero cells resulted in improved production yield. Nucleotide sequence analysis of the IRES revealed five nucleotide changes in Vero cell-adapted RG-HAV (**Fig. 5A and B**). Notably, a substitution from AA to GC at positions 323–324 in the IRES is likely to alter RNA conformation. Additionally, RG-HAV employs optimized codons in its capsid proteins. These conformational changes in the IRES RNA, combined with codon optimization, appear to be associated with enhanced replication and a subsequent increase in the production yield of RG-HAV. Previous reports have demonstrated that the serial passage of HM-175 in FRhK-4 cells under cellular transcription shutoff using actinomycin D generated a fast-growing strain, HM-175-HP [38]. This strain adjusted the codon usage towards a more optimized form. Furthermore, three nucleotide changes in the IRES (U359C, U590C, and U726C) altered the loop connecting IRES domains IV and V, resulting in improved IRES activity compared to HM-175. These findings suggest that altering codon usage in capsid proteins along with enhancing IRES activity through structural changes represents a promising strategy for generating fast-growing HAV vaccine strains. This study and previous reports support the idea that targeted genetic modifications can significantly improve the efficiency of HAV vaccine production.

Adaptation of the RG-HAV strain to Vero cells resulted in 9 amino acid changes in the structural proteins: VP3-T590K; VP1-N982D, S1016P, T1017N, V1018E, and T1019S; and 2A-K1092N,

I1103M, and T1202A (**Fig. 5B**). Importantly, these changes did not occur within the antigenic epitope regions (**Fig. 5C**). Furthermore, immunization with inactivated RG-HAV combined with alum induced an HAV-specific antibody response in mice (**Fig. 6**), demonstrating that these amino acid changes did not affect immunogenicity. The capsid proteins of HAV are vital not only for immunogenicity but also for other functions, such as receptor binding and infectivity. Therefore, it is important to investigate whether amino acid changes in the capsid proteins of RG-HAV influence these functions. This research could provide valuable insights into the HAV life cycle and have significant implications for improving HAV production and developing novel vaccine strains. Future studies should focus on these aspects to further understand the impact of these mutations and to optimize HAV vaccine development.

In summary, the RG-HAV strain generated in this study demonstrated significantly enhanced production yields compared to traditional strains and showed potential for advancing hepatitis A vaccine development. Its improved growth in both Vero and MRC-5 cells and effective immunogenic response in mice during preclinical testing suggest that RG-HAV can substantially improve vaccine production efficiency and reduce costs. This advancement has important implications for meeting the global vaccine demand and ensuring broader access, particularly in low-resource settings.

ACKNOWLEDGMENTS

We thank Professor Myeong Jin Jong at Jeonbuk National University for his technical advice on reverse genetics to generate RG-HAV.

ORCID iDs
Sang Hwan Seo
https://orcid.org/0000-0002-4518-8858
Jung-ah Choi
https://orcid.org/0000-0003-2381-7374
Mi Sun Kim
https://orcid.org/0009-0008-1872-2059
Eunji Yang
https://orcid.org/0000-0003-2590-4551
Sumin Choi
https://orcid.org/0009-0000-2171-3331
Dong Won Seo
https://orcid.org/0000-0001-5299-5183
Manki Song
https://orcid.org/0000-0002-8279-9041

Funding
This study was funded by Andong City and Gyeongsangbuk-do.

Conflict of Interest
No potential conflict of interest relevant to this article was reported.

Author Contributions
Conceptualization: Seo SH, Choi JA; Data curation: Kim MS, Yang E, Choi S; Funding acquisition: Seo DW, Song M; Investigation: Kim MS, Yang E, Choi S; Methodology: Kim MS, Yang E, Choi S; Supervision: Seo DW, Song M; Writing - original draft: Seo SH; Writing - review & editing: Seo SH, Choi JA, Seo DW, Song M.

SUPPLEMENTARY MATERIALS

Supplementary Table 1
Primer sequences used for 3′ or 5′ RACE PCR and sequencing

Supplementary Fig. 1
Morphological changes in MRC-5 and Vero cells after infection with RG-HAV or HM-175.

REFERENCES

1. Wang X, Ren J, Gao Q, et al. Hepatitis A virus and the origins of picornaviruses. Nature 2015;517:85-8. PUBMED | CROSSREF
2. Pintó RM, Pérez-Rodríguez FJ, Costafreda MI, et al. Pathogenicity and virulence of hepatitis A virus. Virulence 2021;12:1174-85. PUBMED | CROSSREF
3. World Health Organization. WHO immunological basis for immunization series: module 18: hepatitis A. Geneva: World Health Organization; 2019.
4. Cao G, Jing W, Liu J, Liu M. The global trends and regional differences in incidence and mortality of hepatitis A from 1990 to 2019 and implications for its prevention. Hepatol Int 2021;15:1068-82. PUBMED | CROSSREF
5. Tjon GM, Coutinho RA, van den Hoek A, et al. High and persistent excretion of hepatitis A virus in immunocompetent patients. J Med Virol 2006;78:1398-405. PUBMED | CROSSREF
6. Severi E, Verhoef L, Thornton L, et al. Large and prolonged food-borne multistate hepatitis A outbreak in Europe associated with consumption of frozen berries, 2013 to 2014. Euro Surveill 2015;20:21192. PUBMED | CROSSREF
7. Garcia Vilaplana T, Leeman D, Balogun K, et al. Hepatitis A outbreak associated with consumption of dates, England and Wales, January 2021 to April 2021. Euro Surveill 2021;26:2100432. PUBMED | CROSSREF
8. Klevens RM, Miller JT, Iqbal K, et al. The evolving epidemiology of hepatitis a in the United States: incidence and molecular epidemiology from population-based surveillance, 2005-2007. Arch Intern Med 2010;170:1811-8. PUBMED | CROSSREF
9. Collier MG, Khudyakov YE, Selvage D, et al. Outbreak of hepatitis A in the USA associated with frozen pomegranate arils imported from Turkey: an epidemiological case study. Lancet Infect Dis 2014;14:976-81. PUBMED | CROSSREF

10. Sane J, MacDonald E, Vold L, Gossner C, Severi E; Outbreak Investigation Team. Multistate foodborne hepatitis A outbreak among European tourists returning from Egypt--need for reinforced vaccination recommendations, November 2012 to April 2013. Euro Surveill 2015;20:21018. PUBMED | CROSSREF
11. Werzberger A, Mensch B, Kuter B, et al. A controlled trial of a formalin-inactivated hepatitis A vaccine in healthy children. N Engl J Med 1992;327:453-7. PUBMED | CROSSREF
12. Xu Z, Wang X, Li R, et al. Immunogenicity and efficacy of two live attenuated hepatitis A vaccines (H(2) strains and LA-1 strains). Zhonghua Yi Xue Za Zhi 2002;82:678-81. PUBMED
13. Shouval D. Immunization against hepatitis A. Cold Spring Harb Perspect Med 2019;9:a031682. PUBMED | CROSSREF
14. European Centre for Disease Prevention and Control (ECDC). Rapid risk assessment: hepatitis A outbreaks in the EU/EEA mostly affecting men who have sex with men, 2nd update, 19 May 2017 [Internet]. Stockholm: ECDC; 2017 [cited 2024 Dec 1]. Available from: https://www.ecdc.europa.eu/en/publications-data/rapid-risk-assessment-hepatitis-outbreaks-eueea-mostly-affecting-men-who-have-0.
15. Petersen J, Freedman J, Ford L, et al. Changes to country-specific hepatitis A travel vaccination recommendation for UK travellers in 2017-responding to a vaccine shortage in the national context. Public Health 2019;168:150-6. PUBMED | CROSSREF
16. Ziesenitz VC, Mazer-Amirshahi M, Zocchi MS, Fox ER, May LSUS. U.S. vaccine and immune globulin product shortages, 2001-15. Am J Health Syst Pharm 2017;74:1879-86. PUBMED | CROSSREF
17. Nelson R. Hepatitis A outbreak in the USA. Lancet Infect Dis 2018;18:33-4. PUBMED | CROSSREF
18. McKnight KL, Lemon SM. Hepatitis A virus genome organization and replication strategy. Cold Spring Harb Perspect Med 2018;8:a033480. PUBMED | CROSSREF
19. Gholizadeh O, Akbarzadeh S, Ghazanfari Hashemi M, et al. Hepatitis A: viral structure, classification, life cycle, clinical symptoms, diagnosis error, and vaccination. Can J Infect Dis Med Microbiol 2023;2023:4263309. PUBMED | CROSSREF
20. Brown EA, Zajac AJ, Lemon SM. *In vitro* characterization of an internal ribosomal entry site (IRES) present within the 5′ nontranslated region of hepatitis A virus RNA: comparison with the IRES of encephalomyocarditis virus. J Virol 1994;68:1066-74. PUBMED | CROSSREF
21. Beales LP, Holzenburg A, Rowlands DJ. Viral internal ribosome entry site structures segregate into two distinct morphologies. J Virol 2003;77:6574-9. PUBMED | CROSSREF
22. Whetter LE, Day SP, Elroy-Stein O, Brown EA, Lemon SM. Low efficiency of the 5′ nontranslated region of hepatitis A virus RNA in directing cap-independent translation in permissive monkey kidney cells. J Virol 1994;68:5253-63. PUBMED | CROSSREF
23. Provost PJ, Giesa PA, McAleer WJ, Hilleman MR. Isolation of hepatitis A virus *in vitro* in cell culture directly from human specimens. Proc Soc Exp Biol Med 1981;167:201-6. PUBMED | CROSSREF
24. Binn LN, Lemon SM, Marchwicki RH, Redfield RR, Gates NL, Bancroft WH. Primary isolation and serial passage of hepatitis A virus strains in primate cell cultures. J Clin Microbiol 1984;20:28-33. PUBMED | CROSSREF
25. Gauss-Müller V, Deinhardt F. Effect of hepatitis A virus infection on cell metabolism *in vitro*. Proc Soc Exp Biol Med 1984;175:10-5. PUBMED | CROSSREF
26. Pintó RM, Pérez-Rodríguez FJ, D'Andrea L, de Castellarnau M, Guix S, Bosch A. Hepatitis A virus codon usage: implications for translation kinetics and capsid folding. Cold Spring Harb Perspect Med 2018;8:a031781. PUBMED | CROSSREF
27. Emerson SU, Huang YK, Purcell RH. 2B and 2C mutations are essential but mutations throughout the genome of HAV contribute to adaptation to cell culture. Virology 1993;194:475-80. PUBMED | CROSSREF
28. Schultz DE, Honda M, Whetter LE, McKnight KL, Lemon SM. Mutations within the 5′ nontranslated RNA of cell culture-adapted hepatitis A virus which enhance cap-independent translation in cultured African green monkey kidney cells. J Virol 1996;70:1041-9. PUBMED | CROSSREF
29. Yi M, Lemon SM. Replication of subgenomic hepatitis A virus RNAs expressing firefly luciferase is enhanced by mutations associated with adaptation of virus to growth in cultured cells. J Virol 2002;76:1171-80. PUBMED | CROSSREF
30. Midthun K, Ellerbeck E, Gershman K, et al. Safety and immunogenicity of a live attenuated hepatitis A virus vaccine in seronegative volunteers. J Infect Dis 1991;163:735-9. PUBMED | CROSSREF
31. Pérez-Rodríguez FJ, D'Andrea L, de Castellarnau M, et al. Improving virus production through quasispecies genomic selection and molecular breeding. Sci Rep 2016;6:35962. PUBMED | CROSSREF
32. Chavarria-Miró G, de Castellarnau M, Fuentes C, et al. Advances for the hepatitis A virus antigen production using a virus strain with codon frequency optimization adjustments in specific locations. Front Microbiol 2021;12:642267. PUBMED | CROSSREF
33. Sun MB, Jiang YJ, Li WD, et al. A novel process for production of hepatitis A virus in Vero cells grown on microcarriers in bioreactor. World J Gastroenterol 2004;10:2571-3. PUBMED | CROSSREF
34. Kiesslich S, Kamen AA. Vero cell upstream bioprocess development for the production of viral vectors and vaccines. Biotechnol Adv 2020;44:107608. PUBMED | CROSSREF
35. Anderson DA. Cytopathology, plaque assay, and heat inactivation of hepatitis A virus strain HM175. J Med Virol 1987;22:35-44. PUBMED | CROSSREF
36. Nasser AM, Metcalf TG. Production of cytopathology in FRhK-4 cells by BS-C-1-passaged hepatitis A virus. Appl Environ Microbiol 1987;53:2967-71. PUBMED | CROSSREF
37. Cromeans T, Fields HA, Sobsey MD. Replication kinetics and cytopathic effect of hepatitis A virus. J Gen Virol 1989;70:2051-62. PUBMED | CROSSREF
38. Aragonès L, Guix S, Ribes E, Bosch A, Pintó RM. Fine-tuning translation kinetics selection as the driving force of codon usage bias in the hepatitis A virus capsid. PLoS Pathog 2010;6:e1000797. PUBMED | CROSSREF